⌘ *Author's Choice*

THE JOURNAL OF BIOLOGICAL CHEMISTRY VOL. 285, NO. 44, pp. 33992–34003, October 29, 2010

Structure of Rpn10 and Its Interactions with Polyubiquitin Chains and the Proteasome Subunit Rpn12*[S]

Received for publication, April 15, 2010, and in revised form, August 3, 2010 Published, JBC Papers in Press, August 24, 2010, DOI 10.1074/jbc.M110.134510

Christiane Riedinger[‡1], Jonas Boehringer[‡1], Jean-Francois Trempe[§1], Edward D. Lowe[‡], Nicholas R. Brown[‡], Kalle Gehring[§], Martin E. M. Noble[‡], Colin Gordon[¶], and Jane A. Endicott[‡2]

From the [‡]Laboratory of Molecular Biophysics, Department of Biochemistry, University of Oxford, South Parks Road, Oxford OX1 3QU, United Kingdom, the [§]Department of Biochemistry, McGill University, 3655 Promenade Sir William Osler, Montreal, Quebec H3G 1Y6, Canada, and the [¶]Medical Research Council Human Genetics Unit, Western General Hospital, Crewe Road, Edinburgh EH4 2XU, Scotland, United Kingdom

Schizosaccharomyces pombe **Rpn10 (SpRpn10) is a proteasomal ubiquitin (Ub) receptor located within the 19 S regulatory particle where it binds to subunits of both the base and lid subparticles. We have solved the structure of full-length SpRpn10 by determining the crystal structure of the von Willebrand factor type A domain and characterizing the full-length protein by NMR. We demonstrate that the single Ub-interacting motif (UIM) of SpRpn10 forms a 1:1 complex with Lys^{48}-linked diUb, which it binds selectively over monoUb and Lys^{63}-linked diUb. We further show that the SpRpn10 UIM binds to SpRpn12, a subunit of the lid subparticle, with an affinity comparable with Lys^{48}-linked diUb. This is the first observation of a UIM binding other than a Ub fold and suggests that SpRpn12 could modulate the activity of SpRpn10 as a proteasomal Ub receptor.**

The post-translational modification of proteins by covalent addition of polyubiquitin chains of diverse length and linkage type is an important mechanism by which cells regulate protein activity. Fidelity in the different pathways regulated by ubiquitylation depends in part on recognition of the character of the modification: Ub[3] may be added to the target protein as a monomer or in chains. Ub chains are distinguished by the identity of the lysine residue within the so-called proximal unit that forms the isopeptide bond with the C-terminal carboxyl group of the neighboring (distal) Ub in the growing Ub chain (1). Proteins that are tagged with linear chains linked through Lys^{48} isopeptide bonds are targeted to the proteasome for degradation (2, 3).

The 26 S eukaryotic proteasome is composed of a 20 S catalytic core and a 19 S regulatory particle (RP). The 19 S RP recognizes the polyUb signal and subsequently brings about substrate deubiquitylation, unfolding, and translocation into the 20 S proteolytic channel (3, 4). The 19 S RP can be subdivided into base and lid subcomplexes (5). The base is composed of 10 subunits: six homologous ATPases that belong to the larger class of AAA (ATPases associated with a variety of cellular activities) ATPases, two scaffold subunits, Rpn1 and Rpn2, and the proteasomal Ub receptors Rpn10 and Rpn13. In contrast, the lid subcomplex contains nine structurally diverse subunits and shares homology with the COP9/signalosome particle in terms of subunit composition and sequence (3, 6).

Rpn10 (first identified as S5a in human cells) and Rpn13/Adrm1 have been identified as proteasomal subunits that act as Ub receptors (7, 8). Rpn13 is associated with Rpn2 and was identified through its ability to mediate recruitment of the deubiquitylating enzyme UCH37 to the proteasome (9). Subsequently, Rpn13 was shown to bind monoUb and polyUb chains via its N-terminal pleckstrin-like receptor for Ub domain (10). Rpn10 interacts with both base (Rpn1/Mts4) and lid (Rpn12/Mts3) subparticles, suggesting a location within the base at the 19 S base/lid interface (5, 11, 12). It is proposed to interact with both Rpn1 and Rpn12 via its N-terminal domain. This domain has weak homology to both the A-domain of the von Willebrand factor (VWA domain), a large multimeric plasma protein that mediates cellular adhesion, and the I-domain of integrins (13). C-terminal to the VWA domain of Rpn10 is an extended Ub binding sequence. Within this region S5a encodes two UIMs (UIM1 and UIM2) (14), whereas the yeast orthologs appear to possess only one, which more closely resembles UIM1 of S5a. As well as being an integral proteasomal subunit, a substantial fraction of Rpn10 can also be isolated from the cytosol (11, 15, 16).

An additional class of Ub receptors exemplified by members of the Rad23/Rhp23 and Dsk2/Dph1 families is not composed of integral proteasome subunits but associates reversibly with it to deliver ubiquitylated substrates for degradation (3, 17, 18). They encode an N-terminal Ub-like domain that binds to Rpn1/Mts4 (12, 19) and one or more ubiquitin-associated domains (UBAs) that confer polyUb binding activity (20, 21).

Recent biophysical studies have begun to elucidate the structural principles that determine the selectivity of different Ub binding domains for Ub chains of different linkage types (22). The human proteasomal Ub receptors HsRpn13 and S5a differ in their affinity and stoichiometry of monoUb and Lys^{48}-linked

* This work was supported by the United Kingdom Medical Research Council, the Canadian Institutes of Health Research, and the Wellcome Trust.

⌘ *Author's Choice*—Final version full access.

[S] The on-line version of this article (available at http://www.jbc.org) contains supplemental Experimental Procedures and additional references, Figs. S1–S6, and Table S1.

The atomic coordinates and structure factors (code 2X5N) have been deposited in the Protein Data Bank, Research Collaboratory for Structural Bioinformatics, Rutgers University, New Brunswick, NJ (http://www.rcsb.org/).

[1] These authors contributed equally to this work.

[2] To whom correspondence should be addressed. Tel.: 441865613290; Fax: +441865613201; E-mail: jane.endicott@bioch.ox.ac.uk.

[3] The abbreviations used are: Ub, ubiquitin; HSQC, heteronuclear single-quantum coherence; ITC, isothermal titration calorimetry; MIDAS, metal ion-dependent adhesion site; RP, regulatory particle; SPR, surface plasmon resonance; UBA, Ub-associated domain; UIM, Ub-interacting motif; VWA, von Willebrand factor type A.

diUb binding. The HsRpn13 pleckstrin-like receptor for Ub domain has a single Ub binding site that binds to Lys^{48}-linked diUb with a 3-fold enhanced affinity over monoUb to generate in each case a 1:1 complex (8). S5a employs its two tandem UIMs to bind monoUb with 1:2 stoichiometry (14) or Lys^{48}-linked diUb to form a 1:1 complex (23). *Schizosaccharomyces pombe* and *Saccharomyces cerevisiae* Rpn10 each encode only a single UIM, and therefore, their binding to Lys^{48}-linked diUb must differ from S5a. In addition, it is not known whether a single UIM can bind selectively to Lys^{48}-linked polyUb chains over other types of chains.

The mechanism by which S5a/Rpn10 binds to both polyUb chains and to the proteasome remains largely unknown. Here, we report a hybrid crystallographic and NMR-derived structure of full-length SpRpn10 and characterize its interaction with polyUb chains and the proteasomal lid subunit SpRpn12. We show that SpRpn10 binds selectively to Lys^{48}-linked diUb with a 1:1 stoichiometry and with a greater affinity than to monoUb or Lys^{63}-linked diUb. NMR experiments show that, in addition to the UIM motif, the linker region between the VWA and UIM sequences is implicated in the binding of Lys^{48}-linked diUb and that both the proximal and distal Lys^{48}-linked Ub moieties contact the single UIM although not simultaneously. We propose that the selectivity of SpRpn10 for Lys^{48}-linked diUb arises from two effects: sterically preferred interchange of UIM binding between the proximal and distal Ubs of Lys^{48}-linked chains, and additional contacts made only by Lys^{48}-linked diUb to the linker sequence that connects the VWA domain and the UIM. We also demonstrate that both the VWA domain and the UIM of SpRpn10 participate in the interaction with SpRpn12, the first indication that UIMs may interact with proteins that do not adopt a Ub fold. The residues of the SpRpn10 UIM that mediate SpRpn12 binding include the conserved LALAL motif that forms the core of the Ub binding site, strongly suggesting that the binding of SpRpn12 and Ub to SpRpn10 are mutually exclusive. SpRpn12 binds to the UIM with an affinity comparable with that of Lys^{48}-linked diUb and considerably higher than monoUb. As such, the interaction of SpRpn12 with the SpRpn10 UIM may "gate" or otherwise modulate access of substrates to the SpRpn10 Ub binding site within the proteasome.

EXPERIMENTAL PROCEDURES

Protein Expression and Purification—An untagged SpRpn10 fragment(1–193) was expressed in *Escherichia coli* and purified by multiple chromatography steps. A more detailed description of the purification procedure is provided in the supplemental Experimental Procedures. SpRpn10 (full-length, residues 1–243), the VWA (1–195) domain and SpRpn12 fragment(1–250) were expressed from pGEX-6P-1 in *E. coli* BL21(DE3) cells and purified by sequential affinity chromatography, 3C protease cleavage and size-exclusion chromatography. Full-length SpRpn10 was grown in LB or $^{15}NH_4Cl$-supplemented and ^{13}C-D-glucose-supplemented M9 minimal medium as required for NMR titrations or assignments. $SpRpn10_{(1-195)}$ was grown in D_2O minimal medium supplemented with $^{15}NH_4Cl$ and $^{2}H^{13}C$-glucose for backbone assignments. Bovine monoUb was purchased from Sigma-Aldrich. Lys^{48}-linked polyUb chains and Lys^{63}-linked diUb were prepared as described (24, 25). Untagged Ub mutants K48C, K63C, and Asp^{77} were constructed using the QuikChange (Stratagene) mutagenesis method and ligation-independent In-Fusion (Clontech) cloning into the pGEX-6P-1 backbone (GE Healthcare). Mutants were purified and then Lys^{48}- and Lys^{63}-linked diUb prepared as described (26). All protein concentrations were determined using extinction coefficients derived from amino acid analysis.

Surface Plasmon Resonance (SPR)—All SPR experiments were conducted on a BIAcore 2000 instrument at 25 °C using HBS-EP buffer (BIAcore). SpRpn10 was diluted to 10 μg ml^{-1} in 10 mM sodium acetate, pH 5.0, and then immobilized at 800 response units on a CM-5 sensor chip by 1-ethyl-3-(3-dimethylaminopropyl)-carbodiimide/*N*-hydroxysuccinimide amine coupling. PolyUb chains were injected over the ligand surface in duplicate at a flow rate of 30 μl min^{-1} for 30s (supplemental Fig. S1*A*). For each analyte concentration, the sensorgram from a mock-immobilization flow cell was subtracted to account for nonspecific binding of the analyte to the CM-5 surface and bulk refractive index change. Steady-state SPR responses were estimated from the subtracted sensorgrams. Affinities were calculated by fitting steady-state responses to a binding isotherm with a Hill coefficient to model the binding of a polyvalent analyte to the ligand.

Isothermal Titration Calorimetry (ITC)—All samples were prepared in 25 mM sodium phosphate, pH 6.5, 50 mM sodium chloride. Concentrations were determined spectrophotometrically at 280 nm using the experimentally determined extinction coefficients of 3,425 $M^{-1}cm^{-1}$ (diUb) and 13,118 $M^{-1}cm^{-1}$ (SpRpn10). All experiments were performed on an iTC200 microcalorimeter (MicroCal) at 25 °C as detailed in the supplemental Experimental Procedures.

Analytical Ultracentrifugation—Samples of Lys^{48}-linked diUb, Lys^{63}-linked diUb, and SpRpn10 were prepared in 25 mM sodium phosphate, pH 6.5, 50 mM sodium chloride. Six concentration ratios of diUb to SpRpn10 ranging from 1:5 to 4:1 were prepared while keeping the total protein concentration constant at 300 μM. Sedimentation velocity experiments were performed in an Optima XL-I (Beckman) analytical ultracentrifuge at 20 °C and 40,000 rpm in an An-60 Ti rotor. $A_{280\ nm}$ measurements were taken at 10-min intervals for a total of 500 min. c(s) analysis for each sample was performed, and the weight-average sedimentation coefficient of each sample was calculated using SEDFIT(27).

X-ray Crystallography Data Collection, Processing, and Structure Solution—A native and a sulfur single wavelength anomalous dispersion dataset were, respectively, collected from the same crystal at the ESRF and in-house. The scaled data from both experiments were used to determine the sulfur sites and to calculate electron density maps with the SHELX suite (28). The initial model was built into the electron density using COOT (29), followed by alternating cycles of refinement in PHENIX.REFINE (30) and manual building in COOT. A more detailed description of the structure solution and refinement is provided in the supplemental Experimental Procedures. The final model comprises residues 2–147 and 151–193, 264 water molecules, and three sulfate ions. 137 (96.48%) residues lie in preferred and 5 (3.52%) in allowed Ramachandran regions.

Data collection and refinement statistics are given in supplemental Table S1.

NMR Spectroscopy: Chemical Shift Titrations with MonoUb, Variously Linked Ub Chains, and SpRpn12—NMR titrations were carried out on home-built GE/Omega spectrometers operating at 11.7, 14.1, and 17.6 T. The concentration of ^{15}N-labeled receptor protein was between 70 and 100 μM, and ^{1}H/^{15}N HSQC spectra were acquired at 0, 25, 50, 75, 100, and 132.5% of ligand, respectively. Titrations with monoUb and Lys^{63}-linked diUb were also repeated with 556 and 140 μM concentrations of ^{15}N-labeled SpRpn10, respectively, and increasing amounts of Ub up to 10-fold excess. Detailed spectral parameters can be found in the supplemental Experimental Procedures.

NMR Assignment—^{2}H,^{13}C,^{15}N-SpRpn10 VWA$_{(1-195)}$ was concentrated to 0.4 mM in 20 mM sodium phosphate, pH 6.0, and 5% D_2O was added. The sample was left to equilibrate for 5 days at room temperature to exchange labile protons. The temperature for all NMR experiments was set to 25 °C unless otherwise stated. HNCACB, HNCA, CBCA(CO)NH, and HN(CO)CA experiments were collected on a 18.7 T (800 MHz) Varian spectrometer. Most residues (~93%) from the VWA domain were assigned using this procedure, with the exception of residues 5, 41, 102–106, 130–133, and 145. To assign residues 192–243, full-length ^{15}N-SpRpn10 was concentrated to 0.1 mM, and 5% D_2O was added and CBCA(CO)NH and CBCANH spectra were acquired on a 500 MHz Bruker spectrometer equipped with a cryoprobe.

Modeling of Full-length SpRpn10 Structure—The structural model of SpRpn10 was prepared by merging the structure of the VWA domain (residues 2–193) with a model of the UIM domain generated with the program esypred3d (31). The modeling is based on sequence alignment with S5a and using the S5a structure (Protein Data Base entry 2KDE) as a template.

RESULTS

Rpn10 Binding to PolyUb Chains—We first set out to characterize the interactions of full-length SpRpn10 with monoUb, Lys^{48}- and Lys^{63}-linked diUb, and Lys^{48}-linked tri- and tetraUb chains. SPR studies (Fig. 1 and supplemental Fig. S1) showed that the binding of SpRpn10 to monoUb is weak, with a measured dissociation constant (K_d) of approximately 130 μM. This value is in agreement with the values for monoUb binding to the individual S5a UIM1 and UIM2 sequences (K_d approximately 350 and 73 μM, respectively) determined by NMR spectroscopy (14, 32). Binding to Lys^{48}-linked diUb was ~5-fold stronger (K_d, approximately 35 μM). Comparison of the observed maximal binding responses (R_{max}) of the analyte and ligand can be used to determine the stoichiometry of complex formation (33). From such an analysis, we find that the UIM of SpRpn10 binds a single Lys^{48}-linked diUb molecule. A significant increase in affinity was observed for binding of Lys^{48}-linked tri- and tetraUb chains. However, in both cases the R_{max} values were not proportional to the number of Ub units in the chain, and the Hill coefficient was much lower than 1. These effects most probably arise from the contribution to binding of a subpopulation of immobilized SpRpn10 molecules that are sufficiently close to each other to engage simultaneously a single molecule of the Lys^{48}-linked tri- or tetraUb analyte, with correspondingly increased apparent affinity. Taking this effect into account, the SPR results suggest a model in which Lys^{48}-linked diUb is the unit of recognition for SpRpn10.

We next characterized the interactions between SpRpn10 and Ub by ITC and sedimentation velocity analytical ultracentrifugation (Fig. 1). ITC confirmed the initial SPR observations: SpRpn10 binds to both monoUb and Lys^{48}-linked diUb with 1:1 stoichiometry and demonstrates a 10-fold preference for binding Lys^{48}-linked diUb (K_d = 13.9 μM) over monoUb (K_d = 139 μM) (Fig. 1). The binding of Lys^{63}-linked diUb to SpRpn10 showed 1:2 stoichiometry and could be modeled by Lys^{63}-linked diUb having two equivalent binding sites for SpRpn10, each with an affinity similar to that of monoUb (134 μM). Analysis of the interaction of SpRpn10 with Lys^{48}- and Lys^{63}-linked diUb by sedimentation velocity analytical ultracentrifugation unambiguously confirmed that Lys^{48}-linked diUb forms a 1:1 complex with SpRpn10 (Fig. 1, *G* and *I*). Analytical ultracentrifugation analysis of the Lys^{63}-linked diUb·SpRpn10 complex yielded a broader profile (Fig. 1, *H* and *I*) that was consistent with the predominant species in solution being a 1:1 complex of relatively weakly binding proteins. It is likely that the 2:1 SpRpn10·Lys^{63}-linked diUb species was not observed by sedimentation velocity analytical ultracentrifugation because the lifetime of this complex is too short for detection by this non-equilibrium method.

To characterize these complexes further, we used NMR spectroscopy and assigned the spectra of both the isolated SpRpn10 VWA domain (supplemental Fig. S2*A*) and the UIM in the context of the full-length protein (supplemental Fig. S2*C*). The more intense resonances of the UIM are not well dispersed but could be visualized separately by choosing a suitable threshold for contouring (supplemental Fig. S2*C*). All residues in the C-terminal UIM-containing sequence (residues 191–241) except Met^{218}, Glu^{220}, and Arg^{222} could be assigned using triple resonance methods.

MonoUb, Lys^{63}-linked diUb, and Lys^{48}-linked diUb were each titrated into SpRpn10 at increasing concentrations up to saturation (Fig. 2). All ligands caused significant chemical shift perturbations in the SpRpn10 spectrum, and in all titrations there was complete broadening for the signals associated with residues 207–208, 210–213, 215–217, 224–225, and 231 (Fig. 2*A*). Notably, residues within the LALAL motif (210–214; Fig. 2*B*) as well as immediately surrounding areas showed line-broadening upon the first addition of ligand. For any ligand, the largest chemical shift changes were found either adjacent to the areas of broadening or in residues 228–230. Titrations of monoUb and Lys^{63}-linked diUb indicated fast chemical exchange on the NMR time scale, whereas titrations of Lys^{48}-linked diUb demonstrated intermediate/slow exchange, consistent with tighter binding (Fig. 2*C*). The largest overall chemical shift changes accompanied addition of Lys^{48}-linked diUb (Fig. 2*A*). Chemical shift changes were smallest in all titrations for residues 235–243 (<0.015 combined chemical shift change), indicating that these residues do not experience a significant change in environment upon polyUb binding.

Addition of monoUb and Lys^{63}-linked diUb resulted in very similar shift patterns within the SpRpn10 C-terminal sequence

A

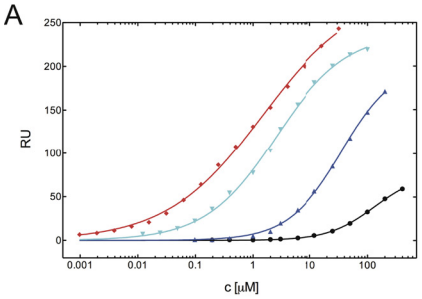

B

Analyte	K_d	R_{max}	Hill Coefficient
Ub	133 ± 7	77.9 ± 1.9	1.07
K48-Ub_2	35.6 ± 2.6	205 ± 5	0.92
K48-Ub_3	2.6 ± 0.2	239 ± 4	0.71
K48-Ub_4	1.5 ± 0.2	288 ± 8	0.52

C

Syringe	Cell	Stoichiometry	K_d [μM]
Ub	SpRpn10	1:1	139 ± 4
K48-Ub_2	SpRpn10	1:1	13.9 ± 0.6
K63-Ub_2	SpRpn10	1:2	134 ± 9

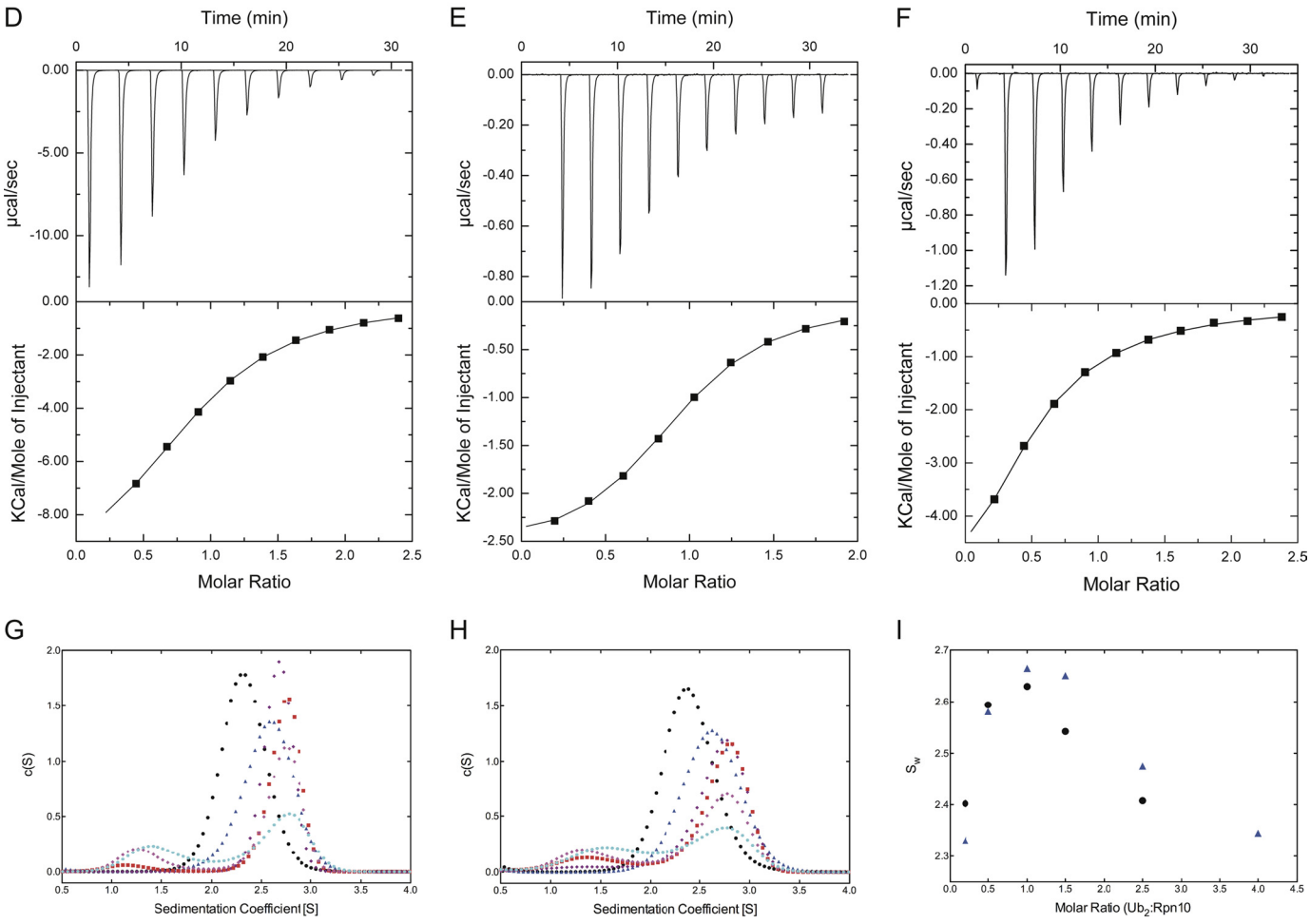

FIGURE 1. **Biophysical characterization of the interactions of SpRpn10 with various Ub chains.** *A*, SPR analysis. SpRpn10 was immobilized by amine coupling to a CM-5 chip, and various polyUb chains (Ub (*black*), Lys^{48}-linked diUb (*blue*), Lys^{48}-linked triUb (*cyan*), and Lys^{48}-linked tetraUb (*red*)) were employed as analytes. Steady-state SPR responses were estimated from the subtracted sensorgrams. *B*, tabulation of respective affinities, R_{max}, and Hill coefficients. *C*, summary of ITC results. *D–F*, ITC analysis. Raw ITC traces with the respective integrated and normalized isotherms of SpRpn10 with monoUb (*D*), Lys^{48}-linked diUb (*E*), and Lys^{63}-linked diUb (*F*). MonoUb and Lys^{48}-linked diUb show 1:1 binding characteristics with affinities of 139 μM and 13.9 μM, respectively. The interaction of Lys^{63}-linked diUb with SpRpn10 can be modeled by a two-site model in which each Ub moiety in Lys^{63}-linked diUb binds Rpn10 with a K_d (134 μM) equivalent to that of monoUb binding. *G–I*, sedimentation velocity analytical ultracentrifugation. Size distribution profiles for each diUb titration are shown in for SpRpn10 and Lys^{48}-linked diUb (*G*) and for SpRpn10 and Lys^{63}-linked diUb (*H*). The total protein concentration was kept constant at 300 μM, and the diUb:SpRpn10 ratio was varied from 0.2 (*black*), 0.5 (*blue*), 1 (*red*), 1.5 (*purple*), 2.5 (*magenta*) to 4.0 (cyan). *I*, plots of the experimentally determined weight-average sedimentation coefficients against the molar ratio. In each case, they indicate formation of a 1:1 complex at the given concentrations. Values for the Lys^{48}- and Lys^{63}-linked diUb titrations are plotted as *blue triangles* and *black circles*, respectively.

(Fig. 2, *C* and *D*). For both ligands, residues 192–206 in the linker sequence experienced little perturbation (<0.05 parts/million), whereas residues 207–232 experienced either larger shifts (>0.05 parts/million) or peak broadening. For all resonances for which a peak could be observed in the bound state, both the direction and magnitude of the chemical shifts were virtually identical (Fig. 2*C*). For Lys^{48}-linked diUb binding, residues 207–232 also experienced shifts in magnitude and direction very similar to those resulting from monoUb or Lys^{63}-linked diUb binding, albeit with intermediate/slow exchange kinetics (Fig. 2*C*). In addition, Lys^{48}-linked diUb caused significant chemical shift changes (>0.05 parts/million) and broadening in the SpRpn10 linker region (residues 192–198 and 201–205) indicative either of a unique interaction in this region or of a conformational change accompanying Lys^{48}-linked diUb binding (Fig. 2, *A* and *E*).

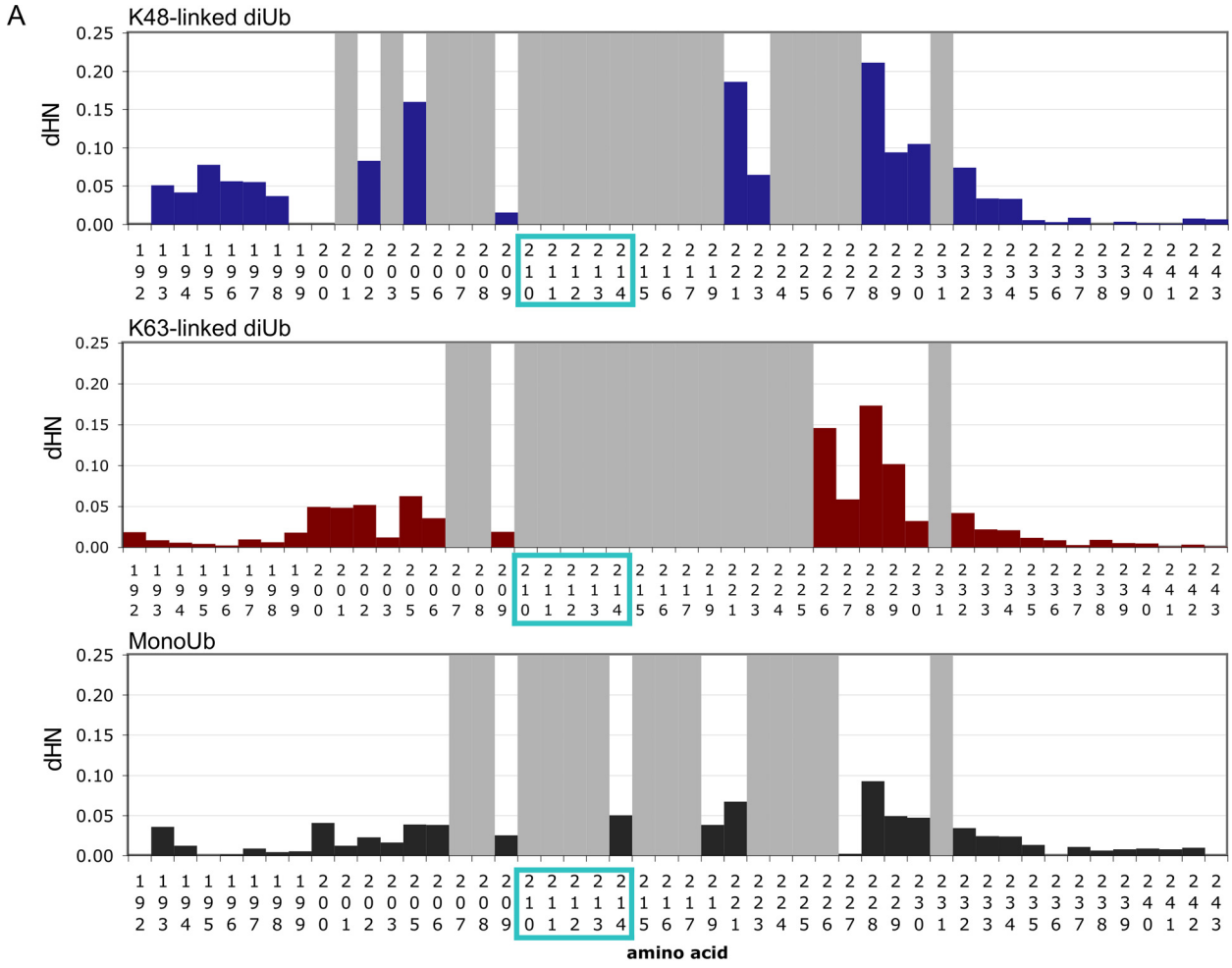
A
K48-linked diUb
K63-linked diUb
MonoUb
dHN
amino acid
B
Sp
Sc
At
Dm
Xl
Rn
Hs
C
228 - MonoUb
228 - K63 diUb
228 - K48 diUb
15N [ppm]
1H [ppm]
D
228 - all
E
192
193
194
196
197

To confirm that both Ub moieties in either Lys^{63}- or Lys^{48}-linked diUb bind to the SpRpn10 UIM, titrations were repeated with diUb in which either the proximal or distal Ub was ^{15}N-labeled, and with ^{15}N-labeled monoUb. Upon SpRpn10 addition, all Ub species undergo significant chemical shift perturbations on the fast/intermediate time scale. Furthermore, line broadening is observed in those residues located at the UIM binding site (centered around Leu^{8}, Ile^{44}, and Val^{70}, Fig. 3). This suggests that both the proximal and distal Ub moieties of both diUbs bind to the UIM. The overall pattern of shifts observed on either monoUb or on the proximal and distal moieties of Lys^{63}-linked diUb are very similar in terms of magnitude, distribution, and signal attenuation. This result suggests that SpRpn10 UIM engages monoUb, or the proximal or distal Ub of Lys^{63}-linked diUb in similar fashion.

Analysis of SpRpn10-induced shifts on Lys^{48}-linked diUb indicated that the proximal unit experiences slightly weaker chemical shift changes than does the distal unit. Furthermore, the distal Lys^{48}-linked diUb experiences larger chemical shift changes in residues 10–12 and 35–39 compared with the other Ub moieties. Notably the C-terminal residues of the distal moiety (involved in the isopeptide bond) undergo severe broadening, which was not observed in the distal moiety of Lys^{63}-linked diUb. However, because most of the spectral changes that accompany SpRpn10 binding are common to the other SpRpn10-Ub titrations, one can conclude that both distal and proximal Ubs of Lys^{48}-linked diUb directly contact the SpRpn10 UIM.

Taken together, our results suggest a model in which SpRpn10 binds equivalently to monoUb or to each of the proximal and distal Ub moieties of Lys^{63}-linked diUb to form either a 1:1 (monoUb·SpRpn10) or 1:2 (Lys^{63}-linked diUb·SpRpn10) complex. Either the distal or proximal Ub of Lys^{48}-linked diUb can also bind to the SpRpn10 UIM. However, in this case binding of one SpRpn10 to either Ub moiety precludes the binding of a second SpRpn10 molecule to the other Ub moiety.

Structural Model of Full-length SpRpn10—SpRpn10 contains an N-terminal VWA domain connected via a short linker to a C-terminal sequence that encodes a single UIM (supplemental Fig. S4). Because attempts to crystallize the full-length protein were not successful, we independently determined the structure of the VWA domain by x-ray crystallography and characterized the UIM by NMR. We identified an untagged construct that encodes SpRpn10 residues 1–193 that crystallized readily (SpRpn10VWA) and solved its structure by sulfur single-wavelength anomalous dispersion at 1.3 Å (supplemental Table S1). The structure consists of a central six-stranded β-sheet of five parallel strands and one antiparallel strand (β3) sandwiched between two triplets of α-helices (Fig. 4*A* and supplemental Fig. S4*C*). The fold and topology are very similar to those of other VWA and I-domains despite their low sequence identities (supplemental Fig. S5).

Between β1 and α1 the Rpn10 VWA domain has a 5-amino acid insertion that is almost invariant among Rpn10 orthologs and is absent in most other VWA domains (Fig. 4 and supplemental Fig. S4). Notably, the insertion disrupts the metal ion-dependent adhesion site (MIDAS) that binds Mg^{2+} ions in a number of VWA domains (34). This part of the VWA fold is essential for maintaining the structural integrity of the 19 S proteasome and for conferring resistance to amino acid analogs (35, 36). Mutation of Asp^{11} at the end of β1 to an arginine results in the dissociation of Rpn3 and other lid subunits, and expression of mutant Rpn10 in which Asp^{11} is converted to any amino acid except glutamate fails to rescue the analog sensitivity of a Δ*rpn10* strain. Substitution by an arginine would not only prevent the formation of a hydrogen bond between the side chain of Asp^{11} and the backbone nitrogen of Gly^{115} (located at the end of β4), but might also disrupt the hydrogen bond between Ser^{13} and Ser^{116}. Together, these changes could result in loss of the loop orientations necessary for interactions with the lid (Fig. 4*B*).

Analysis of the full-length SpRpn10 $^{1}H/^{15}N$ HSQC spectrum shows that the VWA resonances are not perturbed by the presence of the UIM (supplemental Figs. S2 and S3), indicating that the two domains are not in contact with each other. The narrow distribution of UIM peaks in the hydrogen dimension indicates that this region lacks tertiary structure. This interpretation is supported by the fact that no NOE cross-peaks are observed in a three-dimensional $^{1}H/^{15}N$ NOESY-HSQC spectrum that would define contacts between the UIM and other parts of the protein. The sharpness of the UIM peaks result from faster, independent movements of the UIM compared with the VWA domain, so that its resonances are more characteristic of a peptide rather than a 27-kDa protein (supplemental Fig. 2*C*).

Secondary structure prediction algorithms indicate helical propensity in SpRpn10 UIM residues 208–230, consistent with $C\alpha C\beta$ chemical shifts of the UIM obtained from our assignments that indicate a stretch of helical residues between 207 and 228. The structure of the S5a C-terminal tail (14) encodes a helix from residues 214–244 that includes the LALAL motif and corresponds to residues 209–228 in the *S. pombe* ortholog (Fig. 2). Our NMR analysis suggests that there are no other secondary structural elements within the SpRpn10 C-terminal sequence. Taken together, the crystallographic and NMR data suggest a structure for Rpn10 in which a compact VWA fold (residues 1–191) is connected via a long (approximately 16

FIGURE 2. **NMR analysis of the interaction between ^{15}N-labeled SpRpn10 and Ub chains.** *A*, weighted $^{1}H/^{15}N$ chemical shift perturbations in backbone amide HSQC peaks of ^{15}N-SpRpn10 after addition of monoUb, Lys^{63}-linked diUb, or Lys^{48}-linked diUb. Residues for which the peak position in the bound state could not be determined are *highlighted* in *gray*. The position of the LALAL motif that forms the core of the Rpn10 Ub binding site is *boxed* in *cyan*. *B*, Rpn10 sequence alignment. The alignment at the more highly conserved human UIM1 sequence is shown. *Sp*, *S. pombe*; *Sc*, *S. cerevisiae*; *At*, *Arabidopsis thaliana*; *Dm*, *Drosophila melanogaster*; *Xl*, *Xenopus laevis*; *Rn*, *Rattus norvegicus*; *Hs*, *Homo sapiens*. *C*, perturbation of residue 228 of SpRpn10 upon addition of monoUb (*left panel*), Lys^{63}-linked diUb (*center panel*), and Lys^{48}-linked diUb (*right panel*) up to saturation. *D*, overlay of $^{1}H/^{15}N$ HSQC spectra of residue 228 of SpRpn10 in the unbound state (*black*), monoUb-bound (*green*), Lys^{63}-linked diUb-bound (*magenta*), and Lys^{48}-linked diUb-bound (*blue*), highlighting the similarity of chemical shifts in the Ub-bound state. *E*, chemical shift changes of residues 192, 193, 194, 196, and 197, located within the VWA-UIM linker sequence of SpRpn10, upon addition of different Ub chains. Resonances for residues 195 and 198 are in areas of overlap and are therefore not included. For each residue, the apoSpRpn10 resonances are *contoured* in *black*, and those upon addition of 1.3-fold molar excess of monoUb, Lys^{63}- and Lys^{48}-linked diUb are colored *green*, *pink*, and *blue*, respectively.

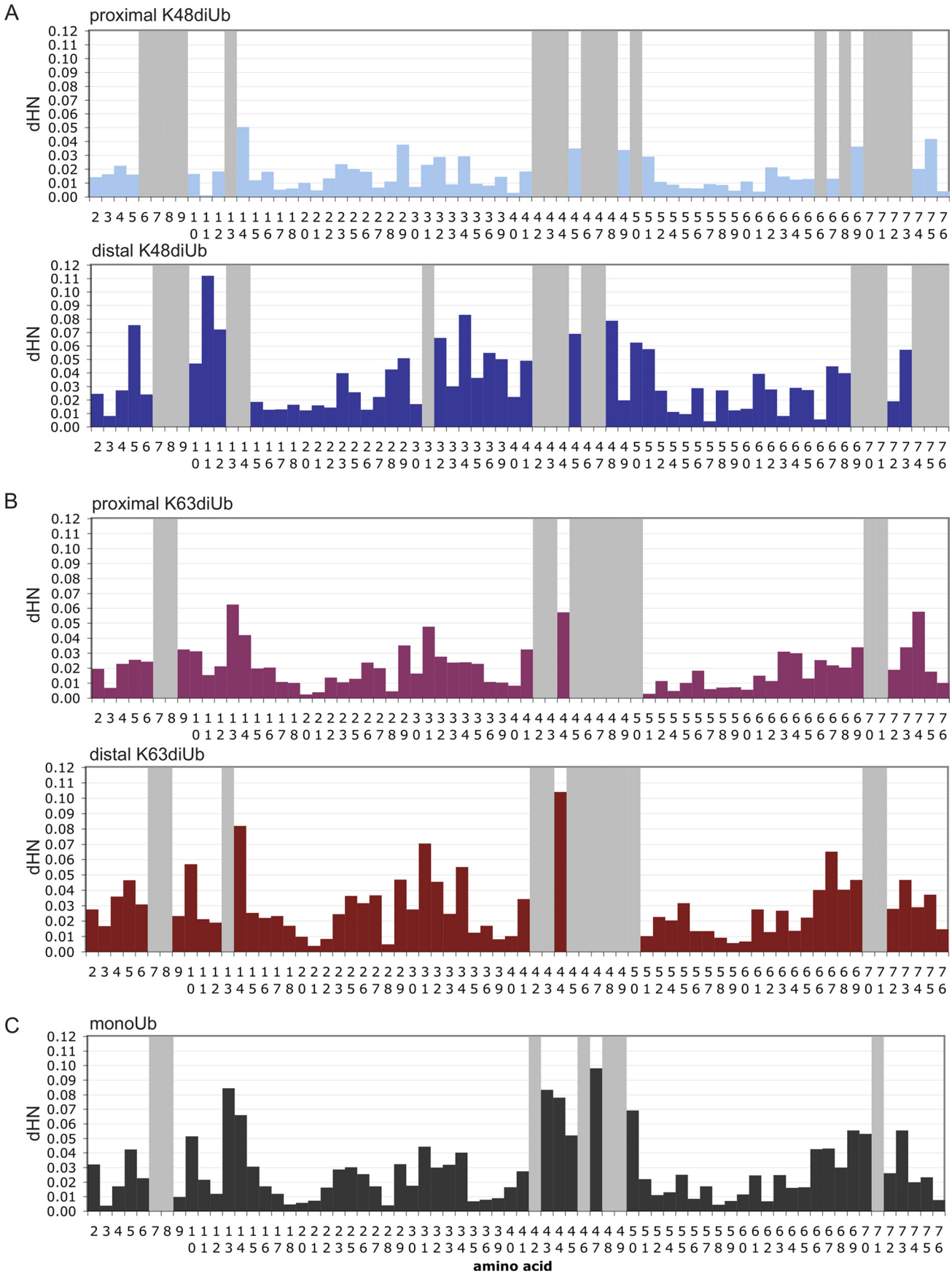

FIGURE 3. **NMR analysis of the interaction between ^{15}N-labeled Ub chains and SpRpn10.** Chemical shift changes were observed in ^{15}N-labeled proximal and distal Lys^{48}-linked diUb (*A*), Lys^{63}-linked diUb (*B*), and monoUb (*C*) at 1.44-fold molar excess of SpRpn10.

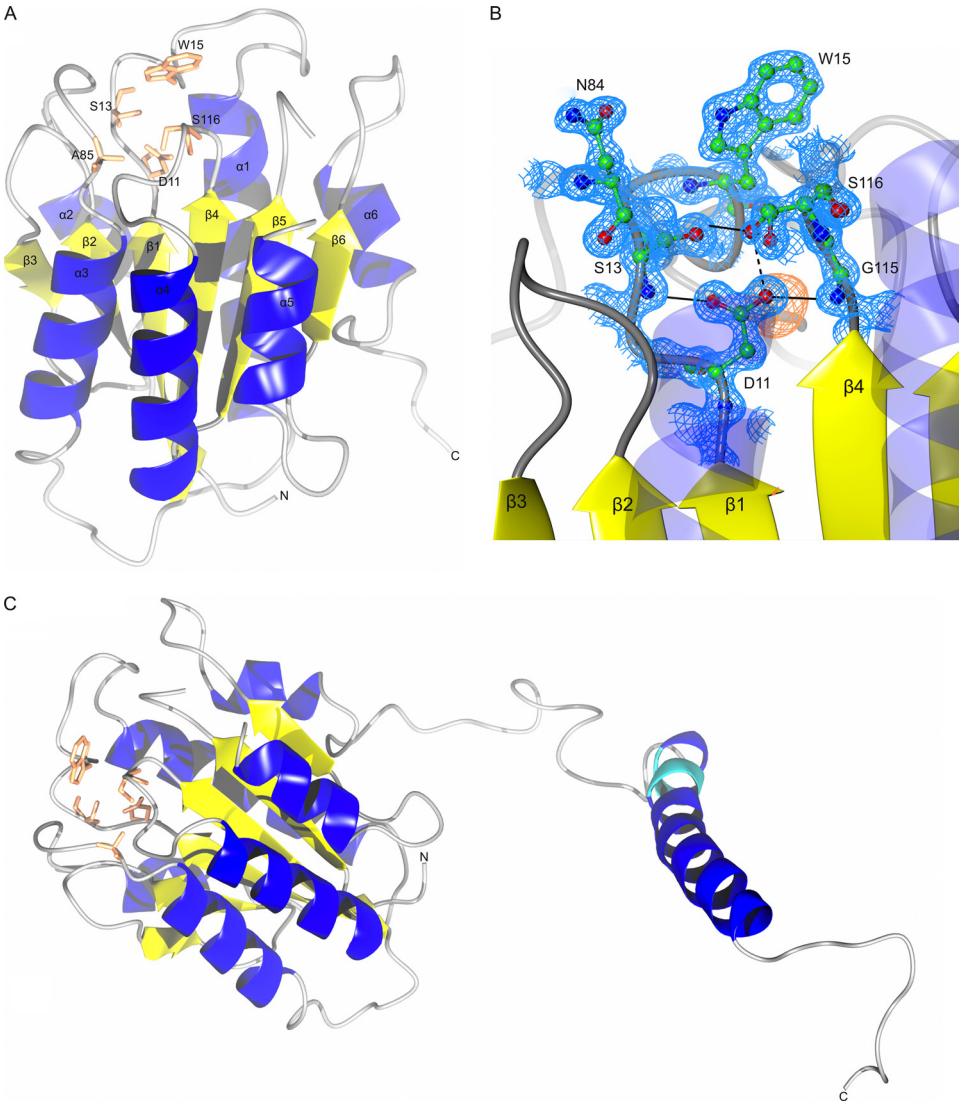

FIGURE 4. **SpRpn10 structure.** *A*, structure of the SpRpn10 VWA domain, drawn with secondary structure elements colored *yellow* (β-sheets β1–β6) and *blue* (α-helices α1–α6). Amino acids that constitute the pseudo-MIDAS motif at the end of β1 are drawn as *cylinders*, labeled, and colored in *coral*. *B*, VWA structure in the vicinity of the pseudo-MIDAS motif. The MIDAS motif is characterized by the sequence D*X*S*X*S together with threonine and aspartate residues in the second (between α2 and α3) and third (between β4 and α4) loops, respectively. In the SpRpn10 VWA domain these residues are replaced by the sequence DNSEW (of which the side chains of Asp[11], Ser[13], and Trp[15] are drawn) and amino acids Ala[85] and Ser[116]. The hydrogen bonds formed by Asp[11] show the importance of interactions in this region for the structural integrity of the "top loop" region of the fold. The $2F_o - F_c$ electron density map is contoured at 0.81 $e^-/Å^3$ and drawn in *blue*, the anomalous difference map at 10.01 $e^-/Å^3$ and colored *orange*. *C*, full-length model of SpRpn10 derived from the VWA crystal structure and the homology-modeled C terminus with the Ub binding LALAL motif *highlighted* in *cyan*.

amino acids), flexible linker to an extended α-helix that in solution does not interact with the VWA domain (Fig. 4*C*).

Interaction of Rpn10 with Rpn12 Involves the VWA Domain and Is Enhanced by Rpn12 Interactions with the UIM—Rpn10 interacts with subunits of the 19 S regulatory particle, located in both the lid (Rpn9, Rpn12) and in the base (Rpt3, Rpn1) subcomplexes (36–38). In fission yeast, deletion of Rpn10 is synthetically lethal with mutations in Rpn12, Rpn11, and Rpn1 (11). We investigated the interaction between SpRpn10 and SpRpn12 in greater detail by performing $^1H/^{15}N$ HSQC titrations exploiting the assigned HSQC spectra of the SpRpn10 VWA domain in isolation and the UIM sequence in the context of the full-length protein (Fig. 5). Upon addition of SpRpn12, the resonances of the SpRpn10 VWA domain show peak disappearance without shifting position, indicative of binding in the slow exchange regime (Fig. 5*A*). Unfortunately, neither addition of saturating amounts of SpRpn12, reacquisition of the spectra at elevated temperatures (up to 40 °C), nor the use of transverse relaxation-optimized spectroscopy could allow us to visualize the VWA signals in the bound state.

However, titration of SpRpn12 into ^{15}N-labeled full-length SpRpn10 revealed chemical shift changes within the UIM domain, indicative of a specific interaction of SpRpn12 with this part of the protein (Fig. 5*B*). Residues on both sides of the LALAL motif showed the largest chemical shift changes in the UIM sequence, whereas the LALAL residues themselves were almost completely broadened upon the first addition of the ligand. A comparative analysis shows that the magnitudes and directions of the UIM chemical shift changes resulting from either SpRpn12 or monoUb titration are different, indicative of the UIM being in distinct environments in each of the bound states (Fig. 5, *C* and *D*). From this analysis, we conclude that the interaction between SpRpn12 and SpRpn10 is mediated unexpectedly by direct interactions between SpRpn12 and the SpRpn10 UIM.

To quantitate the interaction between SpRpn10 and SpRpn12, we measured the change in fluorescence anisotropy accompanying binding of unlabeled $SpRpn10_{196-243}$ to either fluorescently labeled SpRpn12 or, for comparison, fluorescently labeled Lys^{48}-linked diUb (method described in supplemental Experimental Procedures and supplemental Fig. S6). The determined affinities (18 ± 9 μM for SpRpn12 and 9 ± 2 μM for Lys^{48}-linked diUb) demonstrate that the SpRpn10 UIM contributes significantly to the interaction between SpRpn12 and SpRpn10. The close agreement of the affinity of the interactions between Lys^{48}-linked diUb and SpRpn10 when measured by ITC (13.9 μM) and fluorescence anisotropy (9 μM) provides a useful cross-validation of these different techniques.

Competition between SpRpn12 and Ub for Binding to SpRpn10—Because titrations of SpRpn10 with SpRpn12 unexpectedly revealed that the binding sites for SpRpn12 and Ub

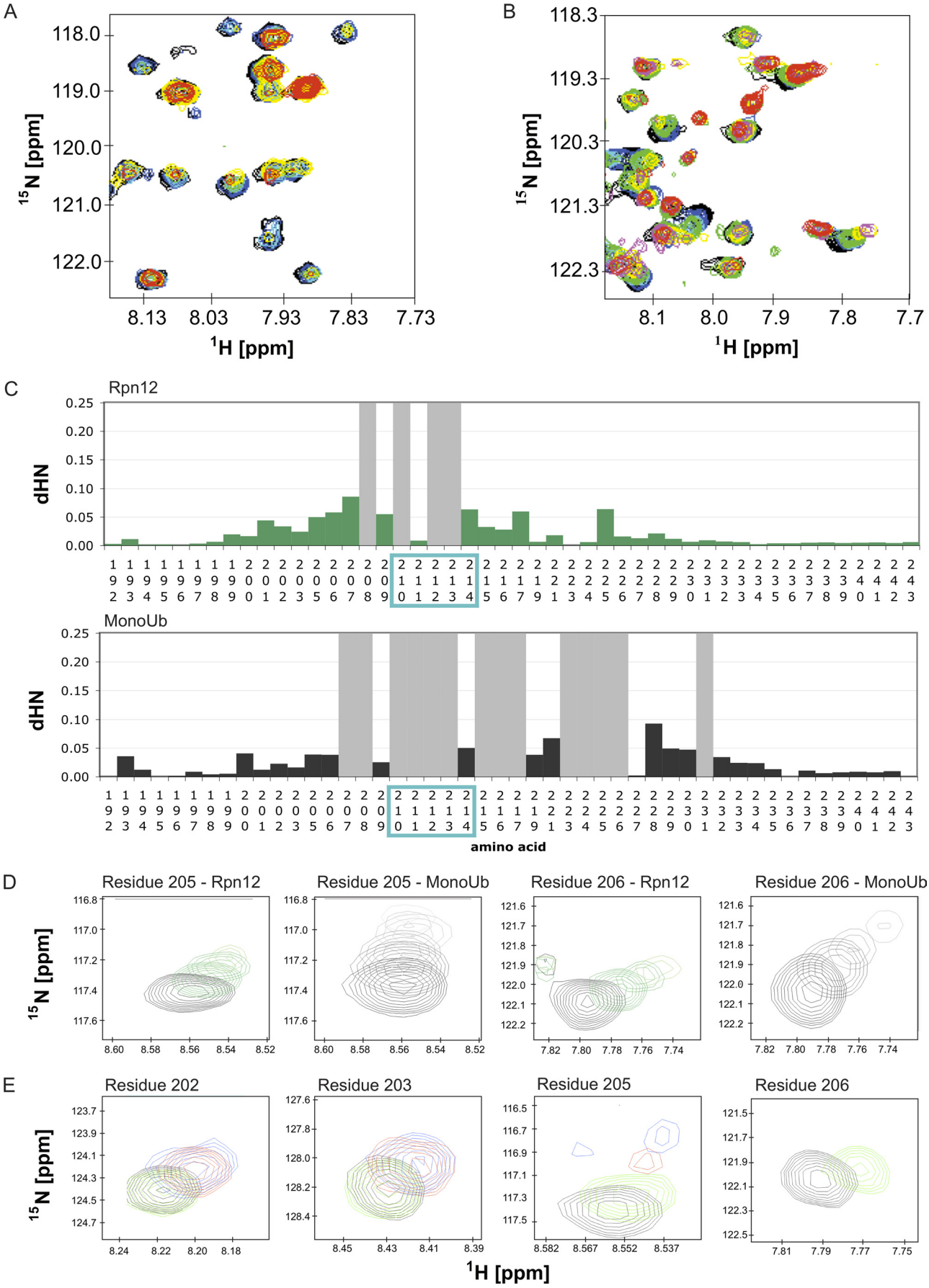
A
B
^{15}N [ppm]
^{1}H [ppm]
C
Rpn12
MonoUb
dHN
amino acid
D
Residue 205 - Rpn12
Residue 205 - MonoUb
Residue 206 - Rpn12
Residue 206 - MonoUb
E
Residue 202
Residue 203
Residue 205
Residue 206

within the SpRpn10 C-terminal sequence overlap, we next carried out competition experiments to determine whether Ub can displace SpRpn12 from SpRpn10. $^{1}H/^{15}N$ HSQC spectra of SpRpn10 were acquired in the SpRpn12-bound state (at 3:1 excess of SpRpn12), in the Lys^{48}-linked diUb-bound state (at 1:1 equimolar concentrations), and at a ratio of 3:1:1 (SpRpn12·Lys^{48}-linked diUb·SpRpn10) (Fig. 5*E*). Analysis of these data indicated that the spectrum of Lys^{48}-linked diUb-bound SpRpn10 is identical to that acquired in the presence of a 3-fold molar excess of SpRpn12. The same result was obtained when the experiment was repeated with a 10-fold molar excess of monoUb. From these data, we conclude that SpRpn12 is released from the UIM in the presence of Lys^{48}-linked diUb or excess monoUb.

DISCUSSION

We have demonstrated that the single UIM present in SpRpn10 binds with low micromolar affinity to Lys^{48}-linked diUb and exhibits approximately 10-fold selectivity for Lys^{48}-linked diUb over Lys^{63}-linked diUb and monoUb. The ITC results demonstrate that SpRpn10 binds Lys^{48}-linked diUb with a 1:1 stoichiometry, and our NMR results show that either the proximal or the distal Ub moiety of Lys^{48}-linked diUb can bind to the SpRpn10 UIM (Fig. 3*A*). In addition, titration of Lys^{48}-linked diUb produces significant chemical shift perturbations and line broadening for residues in the SpRpn10 linker sequence (Val^{192} to Phe^{198} and Gly^{201} to Asn^{205}). A previous NMR study that compared the binding of monoUb and Lys^{48}-linked di- and tetraUb to the ScRpn10 UIM (residues 204–268) concluded that all three Ub molecules contact essentially the same Rpn10 surface (39). Thus, *S. cerevisiae* and *S. pombe* appear to display small differences in the way their Rpn10 linker sequences engage different Ub species.

We generated a model for the Lys^{48}-linked diUb·SpRpn10 complex using our SpRpn10 structure and that of a modeled open conformation of Lys^{48}-linked diUb derived from a closed crystal structure (50) (Fig. 6, *A* and *B*). Binding of the proximal Ub moiety to the LALAL motif of SpRpn10 positions the distal moiety C-terminal to, and on the opposite side of the UIM helix (Fig. 6*A*). Binding of the distal moiety would bring the isopeptide bond and the proximal Ub into close proximity with the SpRpn10 linker and so could account for the Lys^{48} linkage-specific observed chemical shifts in this region. Even though this orientation might be favored, the NMR data support a model in which both alternative binding modes are represented in the bound population. Notably, unlike Lys^{63}-linked diUb, the two UIM binding sites of Lys^{48}-linked diUb face each other so that rebinding is favored. Taken together, the observed shifts in the SpRpn10 linker sequence and the relative positioning of the two Ub UIM binding sites could account for the increased affinity of SpRpn10 for Lys^{48}-linked diUb (Fig. 6).

In contrast, our results demonstrate that both the proximal and distal Ub moieties of Lys^{63}-linked diUb can independently bind to the SpRpn10 UIM employing a binding mode that is essentially indistinguishable from that of monoUb binding. Both monoUb and Lys^{63}-linked diUb bind to ^{15}N-labeled SpRpn10 in fast exchange on the NMR time scale yielding chemical shift perturbations that are similar in their magnitude and direction (Fig. 2). Similarly, observing ^{15}N-proximal or ^{15}N-distal Lys^{63}-linked diUb, the effects of SpRpn10 binding are virtually identical (Fig. 3*B*) to those observed for ^{15}N-monoUb (Fig. 3*C*). The results of the ITC experiments can be rationalized by a model in which the Lys^{63}-linked Ub moieties bind independently to the SpRpn10 UIM with affinities equivalent to that of monoUb to yield a 2:1 complex. We have used our model of full-length SpRpn10 and the structure of Lys^{63}-linked diUb (PDB code 2JF5) to generate a model for the $(SpRpn10)_2$·Lys^{63}-linked diUb complex (Fig. 6*C*). The disposition of the UIM binding sites on opposite sides of the Lys^{63}-linked diUb molecule imposed by the linkage results in both Ub moieties being able to bind independently.

S5a has been shown to bind to Lys^{48}-linked diUb by a mechanism in which both its UIMs simultaneously engage with a different Ub moiety (23). In the most populated structural form of the S5a·Lys^{48}-linked diUb complex, the distal Ub binds to UIM1, and additional interactions are formed between the S5a linker and residues of the distal Ub moiety that are not observed in the S5a·monoUb structure (14). In our proposed model, SpRpn10 may also employ additional interactions with the linker sequence to bind with greater affinity to Lys^{48}-linked diUb. Binding of Lys^{48}-linked diUb to both SpRpn10 and S5a therefore extends the monoUb binding site and provides an explanation for the high degree of sequence conservation between Rpn10 homologs N-terminal to the LALAL motif.

Previous studies of the protein Rap80 have shown that two tandem UIMs can exhibit selectivity for Lys^{63}-linked chains through a mechanism that is exquisitely dependent on the length and properties of the intervening linker region (40–42). Although it has been demonstrated that the single UIM in ScRpn10 binds more tightly to Lys^{48}-linked diUb than to monoUb (39), we believe this to be the first example where Lys^{48}- *versus* Lys^{63}-linkage selectivity has been described and explained for a single UIM. Other Ub binding domains have been found to be linkage-selective. For example, a subset of UBA domains employs a sandwich mechanism to bind selectively to Lys^{48}-linked diUb (24, 43). However, other UBAs have a single Ub binding site and bind monoUb to form 1:1 complexes (44).

Two recent studies have suggested that polyUb chains linked through Lys^{6}, Lys^{11}, and Lys^{29} (45) or Lys^{63} (46) can target substrates to the proteasome. Our results suggest that receptor

FIGURE 5. **SpRpn12 binding to SpRpn10 as observed by NMR spectroscopy.** *A* and *B*, $^{1}H/^{15}N$ HSQC titrations of ^{15}N SpRpn10 VWA (*A*) and UIM and SpRpn12 (*B*) with binding in the slow, intermediate, and fast exchange regime. *Black*, 0%; *blue*, 25%; *cyan*, 50%; *green*, 75%; *yellow*, 175%; *magenta*, 300%; and *red*, 500% SpRpn12. *C*, comparison of the chemical shift changes and line broadening observed upon addition of SpRpn12 (*green*) and monoUb (*black*) mapped onto the primary sequence of the SpRpn10 UIM. Residues for which the peak position in the bound state could not be determined are labeled with the *gray bars*. *D*, chemical shift changes of residues 205 and 206 within the UIM upon addition of SpRpn12 (*green*) and monoUb (*gray*). *E*, selected residues of SpRpn10 in the apo state (*black*), in the presence of 3-fold excess of SpRpn12 (*green*), in the presence of equimolar Lys^{48}-linked diUb (*blue*), and at 1:3:1 ratios of SpRpn10·SpRpn12·Lys^{48}-linked diUb (*red*).

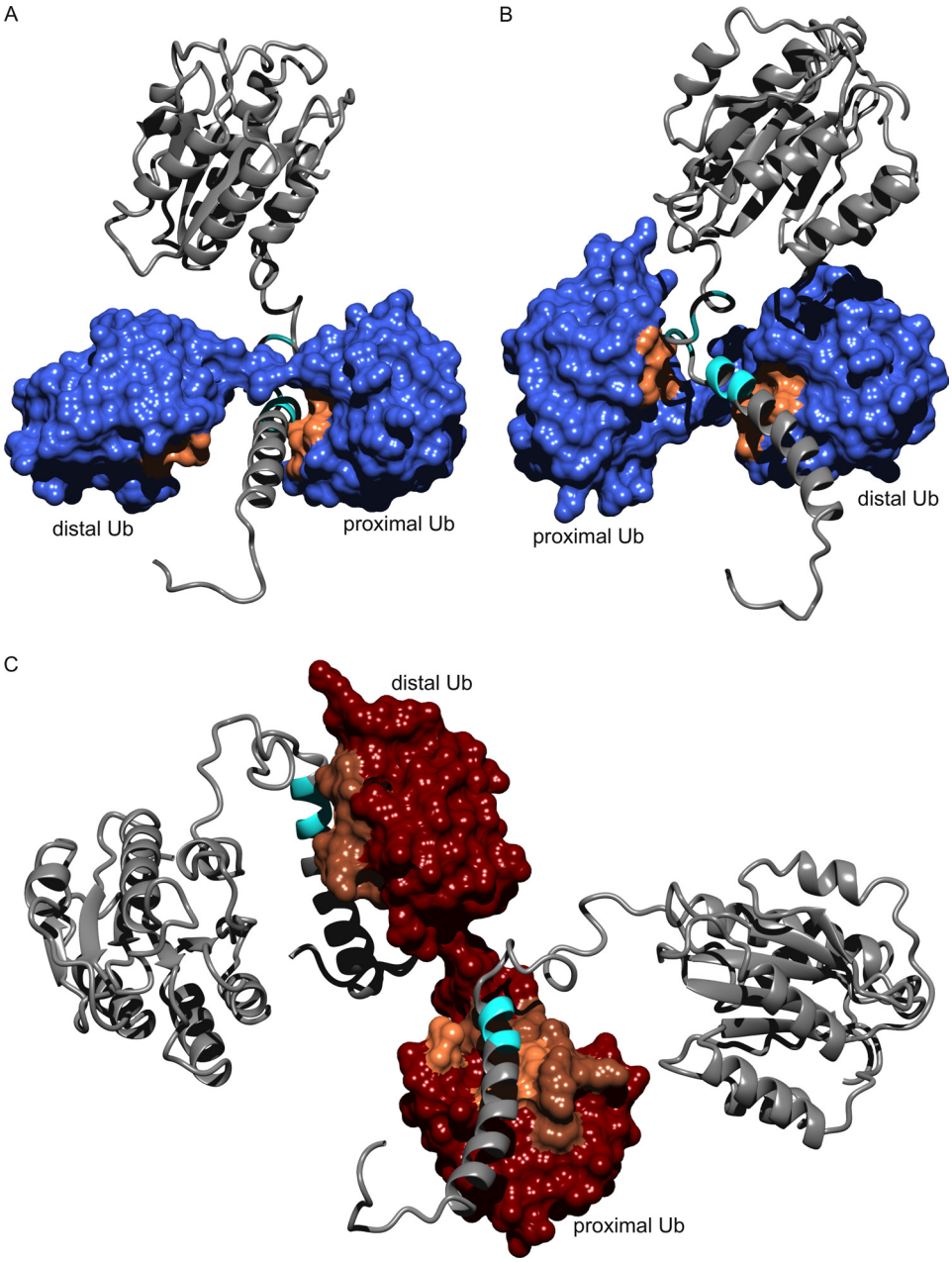

FIGURE 6. **Models for Lys^{48}- and Lys^{63}-linked diUb binding to SpRpn10.** *A*, the two hydrophobic patches of Lys^{48}-linked diUb are facing each other and form a groove that can only accommodate one UIM. With the proximal moiety bound, the distal Ub would be positioned on the opposite side of the UIM helix. *B*, binding of the distal Ub moiety to the UIM places the proximal Ub in close proximity to the SpRpn10 linker region. The groove formed between the two Ub moieties "traps" the UIM between two UIM binding sites, allowing for efficient rebinding. *C*, Lys^{63}-linked diUb is quite extended, and the two hydrophobic UIM binding sites are located on opposite sides of the molecule. This relative disposition permits independent binding of two SpRpn10 molecules. Residues within the SpRpn10 linker sequence that undergo significant chemical shifts upon Lys^{48}-linked diUb binding are colored *dark cyan*. The LALAL motif is colored *cyan*. Ub residues Leu^{8}, Ile^{44}, His^{68}, and Val^{70} which contribute to the UIM binding site are colored *light salmon*. Additional Lys^{63}-linked Ub residues that experience peak broadening upon SpRpn10 addition are colored *dark salmon*.

subunits such as Rpn10 can possess inherent linkage selectivity, suggesting that additional proteasomal receptors may be needed to recruit non-Lys^{48}-linked polyUb chains. We cannot, however, exclude the possibility that Rpn10 acts as a receptor for other polyUb chain types. Although the selectivity for Lys^{48}-linked diUb shown by SpRpn10 is substantial, it is modest compared with the approximately 100-fold selectivity reported for the Lys^{48}-selective Mud1 UBA domain (24), and its affinity for Lys^{48}-linked diUb is low compared with that of Rpn13, another putative proteasome polyUb receptor (8).

Electron microscopy studies of subclasses of 26 S proteasomes suggest that Rpn10 is located close to the mouth of the 19 S RP ATPase module (47). The VWA domain is a protein-protein interaction domain that is found in a variety of signaling pathways, and protein-binding sites have been mapped to various parts of the VWA domain surface (34). The extensive surface conservation of Rpn10 (supplemental Fig. S4) suggests multiple sites of protein interaction compatible with both its proposed location in the 19 S RP and its role as an extraproteasomal Ub receptor. In integrins the MIDAS motif VWA domain undergoes conformational changes upon ligand binding that are transduced to the integrin C-terminal domain so conveying allostery from one end of the domain to the other. Although the MIDAS is not conserved in SpRpn10, protein binding to the equivalent surface on the Rpn10 VWA domain either within the proteasome or in the cytoplasm might transduce an allosteric signal.

A recent report has identified four lysine residues in ScRpn10 (lysines 71, 84, 99, and 268) that undergo monoubiquitylation in response to stress (48). Lys^{84} was identified as the major site and its modification inhibits the ability of the ScRpn10 UIM to bind to substrates. ScRpn10 Lys^{84} is the sequence equivalent of SpRpn10 Asn^{84} that is located in the α2–α3 loop close to the pseudo-MIDAS sequence (Fig. 4) but is not conserved across species (supplemental Fig. S4). Indeed, no surface-exposed lysine residue that is conserved across species lies close in the three-dimensional structure to the site of regulatory modification in ScRpn10. Thus, it remains to be determined to what extent Rpn10 monoubiquitylation is a conserved mechanism regulating its activity across species.

Unexpectedly, we have shown that SpRpn12 interacts with both the UIM and the VWA domains of SpRpn10. The intermolecular masking of the Rpn10 UIM within the proteasome by interaction with SpRpn12 is reminiscent of the intramolecular masking of the hHR23a UBA domains by its Ub-like domain

(49), binding of the ScRpn10 UIM to the Dsk2 Ub-like domain (39), and the recently described masking of the ScRpn10 UIM by VWA monoubiquitylation (48). Our results suggest that modulation of the accessibility of the Ub binding sites of Ub receptors to Ub might be a more widely employed mechanism that would offer an opportunity to regulate the processing of ubiquitylated substrates by the ubiquitin proteasome system.

Acknowledgments—We thank the staff at the ESRF (beamlines ID14-2) for providing excellent facilities and for assistance during data collection. We thank J. Boyd and N. Soffe for NMR facilities; A. Willis for protein analysis; I. Taylor for technical assistance; and C. Khoudian, J. Dean, I. Vakonakis, R. Gilbert, N. Solcan, and J. McDonnell for assistance and useful discussions. We thank D. Barford and D. Komander for constructs.

REFERENCES

1. Dikic, I., Wakatsuki, S., and Walters, K. J. (2009) *Nat. Rev. Mol. Cell Biol.* **10,** 659–671
2. Thrower, J. S., Hoffman, L., Rechsteiner, M., and Pickart, C. M. (2000) *EMBO J.* **19,** 94–102
3. Finley, D. (2009) *Annu. Rev. Biochem.* **78,** 477–513
4. Murata, S., Yashiroda, H., and Tanaka, K. (2009) *Nat. Rev. Mol. Cell Biol.* **10,** 104–115
5. Glickman, M. H., Rubin, D. M., Coux, O., Wefes, I., Pfeifer, G., Cjeka, Z., Baumeister, W., Fried, V. A., and Finley, D. (1998) *Cell* **94,** 615–623
6. Pick, E., Hofmann, K., and Glickman, M. H. (2009) *Mol. Cell* **35,** 260–264
7. Deveraux, Q., Ustrell, V., Pickart, C., and Rechsteiner, M. (1994) *J. Biol. Chem.* **269,** 7059–7061
8. Husnjak, K., Elsasser, S., Zhang, N., Chen, X., Randles, L., Shi, Y., Hofmann, K., Walters, K. J., Finley, D., and Dikic, I. (2008) *Nature* **453,** 481–488
9. Yao, T., Song, L., Xu, W., DeMartino, G. N., Florens, L., Swanson, S. K., Washburn, M. P., Conaway, R. C., Conaway, J. W., and Cohen, R. E. (2006) *Nat. Cell Biol.* **8,** 994–1002
10. Schreiner, P., Chen, X., Husnjak, K., Randles, L., Zhang, N., Elsasser, S., Finley, D., Dikic, I., Walters, K. J., and Groll, M. (2008) *Nature* **453,** 548–552
11. Wilkinson, C. R., Ferrell, K., Penney, M., Wallace, M., Dubiel, W., and Gordon, C. (2000) *J. Biol. Chem.* **275,** 15182–15192
12. Seeger, M., Hartmann-Petersen, R., Wilkinson, C. R., Wallace, M., Samejima, I., Taylor, M. S., and Gordon, C. (2003) *J. Biol. Chem.* **278,** 16791–16796
13. Whittaker, C. A., and Hynes, R. O. (2002) *Mol. Biol. Cell* **13,** 3369–3387
14. Wang, Q., Young, P., and Walters, K. J. (2005) *J. Mol. Biol.* **348,** 727–739
15. van Nocker, S., Sadis, S., Rubin, D. M., Glickman, M., Fu, H., Coux, O., Wefes, I., Finley, D., and Vierstra, R. D. (1996) *Mol. Cell Biol.* **16,** 6020–6028
16. Fu, H., Sadis, S., Rubin, D. M., Glickman, M., van Nocker, S., Finley, D., and Vierstra, R. D. (1998) *J. Biol. Chem.* **273,** 1970–1981
17. Chen, L., and Madura, K. (2002) *Mol. Cell Biol.* **22,** 4902–4913
18. Funakoshi, M., Sasaki, T., Nishimoto, T., and Kobayashi, H. (2002) *Proc. Natl. Acad. Sci. U.S.A.* **99,** 745–750
19. Elsasser, S., Gali, R. R., Schwickart, M., Larsen, C. N., Leggett, D. S., Müller, B., Feng, M. T., Tübing, F., Dittmar, G. A., and Finley, D. (2002) *Nat. Cell Biol.* **4,** 725–730
20. Wilkinson, C. R., Seeger, M., Hartmann-Petersen, R., Stone, M., Wallace, M., Semple, C., and Gordon, C. (2001) *Nat. Cell Biol.* **3,** 939–943
21. Rao, H., and Sastry, A. (2002) *J. Biol. Chem.* **277,** 11691–11695
22. Winget, J. M., and Mayor, T. (2010) *Mol. Cell* **38,** 627–635
23. Zhang, N., Wang, Q., Ehlinger, A., Randles, L., Lary, J. W., Kang, Y., Haririnia, A., Storaska, A. J., Cole, J. L., Fushman, D., and Walters, K. J. (2009) *Mol. Cell* **35,** 280–290
24. Trempe, J. F., Brown, N. R., Lowe, E. D., Gordon, C., Campbell, I. D., Noble, M. E., and Endicott, J. A. (2005) *EMBO J.* **24,** 3178–3189
25. Komander, D., Lord, C. J., Scheel, H., Swift, S., Hofmann, K., Ashworth, A., and Barford, D. (2008) *Mol. Cell* **29,** 451–464
26. Pickart, C. M., and Raasi, S. (2005) *Methods Enzymol.* **399,** 21–36
27. Schuck, P., and Rossmanith, P. (2000) *Biopolymers* **54,** 328–341
28. Sheldrick, G. M. (2008) *Acta Crystallogr. Sect. A* **64,** 112–122
29. Emsley, P., and Cowtan, K. (2004) *Acta Crystallogr. D Biol. Crystallogr.* **60,** 2126–2132
30. Adams, P. D., Grosse-Kunstleve, R. W., Hung, L. W., Ioerger, T. R., McCoy, A. J., Moriarty, N. W., Read, R. J., Sacchettini, J. C., Sauter, N. K., and Terwilliger, T. C. (2002) *Acta Crystallogr. D Biol. Crystallogr.* **58,** 1948–1954
31. Lambert, C., Léonard, N., De Bolle, X., and Depiereux, E. (2002) *Bioinformatics* **18,** 1250–1256
32. Ryu, K. S., Lee, K. J., Bae, S. H., Kim, B. K., Kim, K. A., and Choi, B. S. (2003) *J. Biol. Chem.* **278,** 36621–36627
33. Morton, T. A., and Myszka, D. G. (1998) *Methods Enzymol.* **295,** 268–294
34. Springer, T. A. (2006) *Structure* **14,** 1611–1616
35. Glickman, M. H., Rubin, D. M., Fu, H., Larsen, C. N., Coux, O., Wefes, I., Pfeifer, G., Cjeka, Z., Vierstra, R., Baumeister, W., Fried, V., and Finley, D. (1999) *Mol. Biol. Rep.* **26,** 21–28
36. Fu, H., Reis, N., Lee, Y., Glickman, M. H., and Vierstra, R. D. (2001) *EMBO J.* **20,** 7096–7107
37. Drews, O., Zong, C., and Ping, P. (2007) *Proteomics* **7,** 1047–1058
38. Taverner, T., Hernández, H., Sharon, M., Ruotolo, B. T., Matak-Vinkoviæ, D., Devos, D., Russell, R. B., and Robinson, C. V. (2008) *Acc. Chem. Res.* **41,** 617–627
39. Zhang, D., Chen, T., Ziv, I., Rosenzweig, R., Matiuhin, Y., Bronner, V., Glickman, M. H., and Fushman, D. (2009) *Mol. Cell* **36,** 1018–1033
40. Sato, Y., Yoshikawa, A., Mimura, H., Yamashita, M., Yamagata, A., and Fukai, S. (2009) *EMBO J.* **28,** 2461–2468
41. Walters, K. J., and Chen, X. (2009) *EMBO J.* **28,** 2307–2308
42. Sims, J. J., and Cohen, R. E. (2009) *Mol. Cell* **33,** 775–783
43. Varadan, R., Assfalg, M., Raasi, S., Pickart, C., and Fushman, D. (2005) *Mol. Cell* **18,** 687–698
44. Ohno, A., Jee, J., Fujiwara, K., Tenno, T., Goda, N., Tochio, H., Kobayashi, H., Hiroaki, H., and Shirakawa, M. (2005) *Structure* **13,** 521–532
45. Xu, P., Duong, D. M., Seyfried, N. T., Cheng, D., Xie, Y., Robert, J., Rush, J., Hochstrasser, M., Finley, D., and Peng, J. (2009) *Cell* **137,** 133–145
46. Saeki, Y., Kudo, T., Sone, T., Kikuchi, Y., Yokosawa, H., Toh-e, A., and Tanaka, K. (2009) *EMBO J.* **28,** 359–371
47. Nickell, S., Beck, F., Scheres, S. H., Korinek, A., Förster, F., Lasker, K., Mihalache, O., Sun, N., Nagy, I., Sali, A., Plitzko, J. M., Carazo, J. M., Mann, M., and Baumeister, W. (2009) *Proc. Natl. Acad. Sci. U.S.A.* **106,** 11943–11947
48. Isasa, M., Katz, E. J., Kim, W., Yugo, V., González, S., Kirkpatrick, D. S., Thomson, T. M., Finley, D., Gygi, S. P., and Crosas, B. (2010) *Mol. Cell* **38,** 733–745
49. Walters, K. J., Lech, P. J., Goh, A. M., Wang, Q., and Howley, P. M. (2003) *Proc. Natl. Acad. Sci. U.S.A.* **100,** 12694–12699
50. Trempe, J.-F., Brown, N. R., Noble, M. E., and Endicott, J. A. (2010) *Acta Crystallogr. Sect. F Struct. Biol. Cryst. Commun.* **66,** 994–998